2013 IEEE 10th International Symposium on Biomedical Imaging:
From Nano to Macro
San Francisco, CA, USA, April 7-11, 2013

DIFFEOMORPHIC POINT SET REGISTRATION USING NON-STATIONARY MIXTURE MODELS

D. Wassermann, J. Ross, G. Washko, C-F Westin, R. San José Estépar

Brigham and Women's Hospital, Harvard Medical School, Boston, MA, USA

ABSTRACT

This paper investigates a diffeomorphic point-set registration based on non-stationary mixture models. The goal is to improve the non-linear registration of anatomical structures by representing each point as a general non-stationary kernel that provides information about the shape of that point. Our framework generalizes work done by others that use stationary models. We achieve this by integrating the shape at each point when calculating the point-set similarity and transforming it according to the calculated deformation. We also restrict the non-rigid transform to the space of symmetric diffeomorphisms. Our algorithm is validated in synthetic and human datasets in two different applications: fiber bundle and lung airways registration. Our results shows that non-stationary mixture models are superior to Gaussian mixture models and methods that do not take into account the shape of each point.

1. INTRODUCTION

Point-set based representations arise in a wide variety of medical imaging applications. Examples include the extraction of airways, bones, and white matter tracts [1, 2, 3]. The ability to register two different point-sets representing the same anatomical structure is critical to the statistical study of different pathologies. Non-rigid point-set registration algorithms exist (e.g. [4, 5]); however, these algorithms represent structures as a collection of points in $\mathbb{R}^3$ neglecting valuable information regarding the shape of the structure, e.g. the thickness of the trachea. In this work we generalize point-set registration by endowing points with kernel functions that encode either shape (e.g. tube or ellipsoid) or uncertainty in physical location. We refer to these data sets as *shaped particles*.

When spatially aligning two anatomical structures, it is desirable that the transformations be *diffeomorphic* [6, 7] and *symmetric* [7, 8]. Restricting the transform to a *diffeomorphism* preserves the topology of the registered structure, prevents the transform from introducing foldings which are often physically impossible, and guarantees that the transform is invertible. *Symmetry* guarantees that the resulting transform is identical regardless of input ordering, making the obtained transformations more appropriate for further statistical analyses [7, 8]. To the best of our knowledge, algorithms that obtain non-rigid transforms between unlabeled point-sets disregard the diffeomorphic [5, 9] and symmetry constraints[10].

Our contribution in this paper is twofold. Unlike [4, 5], we present a registration algorithm with a non-stationary calculation of the point-set similarity by using a different kernel function for each point. The point-set is in turn represented by a mixture of kernels. The goal is to minimize the discrepancy measurement between the mixture models of the point sets that are being registered. Framing the problem in this way enables us to utilize information about structure co-dimensionality and thus achieve more accurate registrations. Second, our algorithm guarantees that the resulting non-rigid transform is diffeomorphic and symmetric.

We evaluate our registration algorithm on synthetic data sets and data sets derived from human airway trees and white matter fiber tracts. We show results of the registration of a set of subjects to illustrate the performance of our method and its applicability to population-based studies. We show the utility of our technique by performing a statistical analysis on the transforms of two airway sets, and characterize differences in subjects with chronic obstructive pulmonary disease (COPD).

2. METHODS

2.1. Point-set Dense Representation in Space

Let $P = \{\mathbf{p}_1, \ldots, \mathbf{p}_N\}$ be a shaped particle data set distributed on the centerline or surface of an anatomical structure $\mathcal{S}$. Each shaped particle is given by $\mathbf{p}_i = (\mathbf{c}_i, \theta_i)$, where $\mathbf{c}_i \in \mathbb{R}^3$ is the center of the particle, and θ_i are the parameters of the shape. We represent the density of particles at each point in space as a mixture of shaped kernel functions

$$d(\mathbf{x}) = z \sum_{i=1}^{N} K_i(\mathbf{p}_i, \mathbf{x}) \tag{1}$$

where $K_i(\cdot,\cdot)$ is a positive definite kernel defined at each $\mathbf{c}_i$ with shape defined by parameters θ_i, and z is a normalization constant ensuring $\int d(\mathbf{x})d\mathbf{x} = 1$. We next define the inner product between two shaped particle sets as the L_2 inner product between density functions:

$$\langle P_1, P_2\rangle := \langle d_1, d_2\rangle = \int d_1(\mathbf{x})d_2(\mathbf{x})d\mathbf{x} = z_1 z_2 \sum_{ij} \int K_{1_i}(\mathbf{p}_{1_i}, \mathbf{x})K_{2_j}(\mathbf{p}_{2_j}, \mathbf{x})d\mathbf{x}. \tag{2}$$

Funded by NIH: 1R01HL116931, R01MH092862, R01MH074794, P41EB015902, K25HL104085, K23HL089353

leading to a similarity measure between particle sets:

$$\mathrm{cor}(P_1, P_2) = \mathrm{cor}(d_1, d_2) = 1 - \frac{\langle d_1, d_2 \rangle^2}{\langle d_1 \rangle \langle d_2 \rangle} \tag{3}$$

This similarity measure has been shown to have a rich number of mathematical interpretations which are generalizable to the shaped particle case. As $d(\mathbf{x})$ in eq. (1) is a density function, $\mathrm{cor}(\cdot,\cdot)$ is proportional to Renyi's Quadratic Entropy [4] and a special case of the power divergence between two probability densities [5]. From the robust statistics point of view, it is equivalent to an M-Estimator on the point-to-point distances between the particle sets [4]. Inscribing the similarity measure in such mathematical frameworks not only broadens its interpretation, but opens the door to studying its robustness with respect to noise. Having presented our similarity measure for shaped particle sets, we present a symmetric diffeomorphic registration algorithm.

2.2. Registration of Particle-Sets

When registering two shaped particle sets, we look for a transform which, when applied to the set P_1 maps it to a set having a high resemblance with P_2: we search for the map $\phi : \mathbb{R}^3 \mapsto \mathbb{R}^3$ such that $\phi(P_1) := \{\phi(\mathbf{p}_{1_i})\}_{i=1\ldots N} \sim P_2$.

As stated earlier, we seek a transformation that is symmetric and diffeomorphic. The parameters of such a transform, ϕ, are 1) a coordinate $\mathbf{x}$; 2) a time $t \in [0,1]$ such that $\phi(\cdot,0) = \mathbf{Id}$, $\phi(P_1,1) \sim P_2$ and $\phi^{-1}(P_2,1) \sim P_1$; and 3) a velocity field $\mathbf{v}(\mathbf{x},t)$ such that we calculate ϕ integrating $\mathbf{v}$ along time: $\phi(\mathbf{x},1) = \phi(\mathbf{x},0) + \int_0^1 \mathbf{v}(\phi(\mathbf{x},t),t)dt$. The length of the path for $\mathbf{x}$ along the map is $D(\phi(\mathbf{x},0),\phi(\mathbf{x},1)) = \int_0^1 \|\mathbf{v}(\mathbf{x},t)\|_L dt$, where L defines a linear operator regularizing the velocity field. The norm $\|\cdot\|_L$ regularizes the velocity field via the linear difference operator $L = a\nabla + b\,\mathbf{Id}$ where a and b are constants. Then, $\phi(\mathbf{x},t)$, is a diffeomorphism.

We calculate the transform $\phi(\mathbf{x},t)$ using the symmetric diffeomorphic optimizer algorithm described in [7]. We simultaneously look for two maps ϕ_1 and ϕ_2 such that one is the symmetric inverse of the other: $\phi_1(\mathbf{x},t) = \phi_2(\mathbf{z},1-t)$. Combined with the requirement $\phi_1(P_1,1) \sim P_2$, this leads to ϕ_1 and ϕ_2 mapping P_1 to P_2: $\phi_2^{-1}(\phi_1(P_1,t),1-t) \sim P_2$. We compute ϕ_1 and ϕ_2 by minimizing:

$$E(P_1,P_2) = \inf_{\phi_1,\phi_2} \int_0^{\frac{1}{2}} \left\{ \|\mathbf{v}_1(\mathbf{x},t)\|_L^2 + \|\mathbf{v}_2(\mathbf{x},t)\|_L^2 \right\} dt + \mathrm{cor}(\phi_1(P_1,\tfrac{1}{2}),\phi_2(P_2,\tfrac{1}{2})) \tag{4}$$

subjecting ϕ_1, ϕ_2 to be a diffeomorphism: $d\phi_i(\mathbf{x},t)/dt = \mathbf{v}_i(\phi_i(\mathbf{x},t),t)$; $\phi_i(\mathbf{x},0) = \mathbf{Id}$; and $\phi_i(\phi_i^{-1}) = \mathbf{Id}$ and constraining both transformations to having the same length $\|\mathbf{v}_1(\cdot,t)\| = \|\mathbf{v}_2(\cdot,t)\|$. The first term of eq. (4) ensures that ϕ_1 and ϕ_2 are smooth. The second term sets the transforms to map P_1 to P_2 symmetrically by enforcing the similarity of both particle sets deformed half way. The constraint

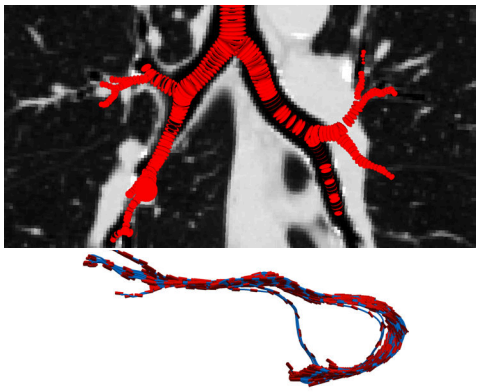

Fig. 1: Illustration of how the particles assume different shapes in different applications. At the top we show the extracted airway with ellipsoidal particles, at the bottom a white matter bundle with tube-shaped particles.

$\phi_1(\mathbf{x},\frac{1}{2}) = \phi_2(\mathbf{x},\frac{1}{2})$ is included in the fact that we integrate the solution from 0 to $\frac{1}{2}$. We minimize this energy using the algorithm presented by Avants et al. [7]. This algorithm produces a smooth invertible map ϕ_1 that will map P_1 to P_2.

To minimize eq. (4) given the specified constraints, we use the following Euler-Lagrange equation for ϕ_1:

$$\nabla_{\phi_1\left(\mathbf{x},\frac{1}{2}\right)} E = 2L\mathbf{v}_1(\mathbf{x},\tfrac{1}{2}) + \frac{2\langle \bar{P}_1, \bar{P}_2 \rangle}{\langle \bar{P}_1 \rangle \langle \bar{P}_2 \rangle} \times \left(\bar{d}_2(\mathbf{x}) - \frac{\langle \bar{P}_1, \bar{P}_2 \rangle}{\langle \bar{P}_2 \rangle} \bar{d}_1(\mathbf{x}) \right) |\mathbf{D}\,\phi_1| \nabla \bar{d}_1(\mathbf{x}) \tag{5}$$

and the gradient w.r.t. ϕ_2 is analogous. In eq. (5), $\bar{P}_i := \phi_i(P_i,\frac{1}{2})$, in which each particle is deformed as $\phi_i(\mathbf{p},\frac{1}{2}) = (\phi_i(\mathbf{c},\frac{1}{2}),\phi_i(\theta,\frac{1}{2}))$, $\bar{d}_i(\mathbf{x})$ is the density function that corresponds to $\bar{P}_i$ and $|\mathbf{D}\,\phi|$ is the Jacobian of the transformation ϕ. The action of the diffeomorphism ϕ over the particle parameters must be defined for each particle type.

2.3. Transformation of the Particle Features

We analyze shape features corresponding to line segments and ellipsoids and consider specific applications

Line segment: When we consider line-shaped particles the feature $\mathbf{f}_i \in \mathbb{R}^3$ is the vector defining the direction and length of the line. We reorient and rescale the particle according to the Jacobian of the transformation $\phi(\mathbf{f}_i) = \mathbf{D}\phi(\mathbf{p}_i)\mathbf{f}_i$.

Ellipsoid: When we consider ellipsoidal-shaped particles the feature is a positive-definite symmetric matrix, $\mathbf{F}_i \in \mathrm{Sym}^3$. We rotate and rescale the ellipsoid according to the deformation $\phi(\mathbf{F}_i) = \mathbf{D}\phi(\mathbf{p}_i)\mathbf{F}_i[\mathbf{D}\phi(\mathbf{p}_i)]^T$.

2.4. Application-Specific Shaped Particles

Airway datasets In the case of our airway datasets, we sample the airway centerline with scale space particles [3]. The particles are equally distributed along the centerline of the airways at a distance s (fig. 1). Such particles have an ellipsoidal

shape. Their minor axis is aligned with the airway's centerline and has a length of s 2. The remaining axes have equal length set to the lumen size of the airway. We define the kernel K_i:

$$K_i(\mathbf{p}_i \ \mathbf{x}) := \exp \quad (\mathbf{x} \quad \mathbf{p}_i)^T \mathbf{F}_i \ ^1 (\mathbf{x} \quad \mathbf{p}_i) \qquad (6)$$

where the smallest eigenvalue of $\mathbf{F}_i$ is set to the inter-particle distance s 2 with its eigenvector aligned with the extracted airway direction, and the other two eigenvalues have the lumen size at $\mathbf{p}_i$ as their magnitude. The feature used to shape the matrix is an ellipsoid represented by F_i Sym^3 which we deform as described in section 2.3. In the limiting case our ellipsoids become infinitely thin, and the ellipsoids are discs reconstructing the tubular structure of the airways.

White Matter Tracts With respect to our white matter tract datasets, we consider the particles shaped as line segments. A white-matter tract particle set P is composed by several subsets $P = \ P^1 \quad P^N$ such that each $P^j = \ \mathbf{p}_1^j \quad \mathbf{p}_{N^j}^j$ represents a curve. Each particle is shaped as a segment such that the feature $\ _i^j$ associated with particle $\mathbf{p}_i^j$ is $\mathbf{f}_i^j = (\mathbf{p}_{i+1}^j \ \mathbf{p}_i^j)$ for $i = 1 \ N^j \quad 1$. Then, the application-specific kernel which represents each white matter tract as a sequence of segments is a function of the distance between the point $\mathbf{x}$ and the distance between that point and the segment $\mathbf{f}_i^j$ at $\mathbf{p}_i^j$:

$$K_i^j(\mathbf{p}_i^j \ \mathbf{x}) := \exp \quad \mathrm{dist}(\mathbf{x} \ \mathbf{f}_i^j) \qquad (7)$$

where $\mathrm{dist}(\mathbf{x} \ \mathbf{f}_i^j)$ is the distance between the point $\mathbf{x}$ and the segment $\mathbf{f}_i^j$:

$$\mathrm{dist}(\mathbf{x} \ \mathbf{f}_i^j) := \begin{array}{lll} \mathbf{p}_i^j \quad \mathbf{x} & & t \quad 0 \\ \mathbf{p}_i^j + t(\mathbf{p}_{i+1}^j \quad \mathbf{p}_i^j) \quad \mathbf{x} & & 0 < t < 1 \\ \mathbf{p}_{i+1}^j \quad \mathbf{x} & & 1 \quad t \end{array}$$

$$t = \frac{(\mathbf{x} \quad \mathbf{p}_i^j) \ (\mathbf{p}_{i+1}^j \quad \mathbf{p}_i^j)}{\mathbf{p}_{i+1}^j \quad \mathbf{p}_i^j \ ^2}$$

We have presented two different applications with differently-shaped particles and kernels. Combining this with our particle-set representation scheme and registration algorithm, we demonstrate our registration algorithm in synthetic and human datasets and show a statistical application using the resulting deformation fields.

3. EXPERIMENTS

Synthetic Experiments Our non-stationary mixture model was compared against the Gaussian mixture model (GMM) based on two implementations: the one originally proposed by [5] (GMM) and an extension based on our symmetric diffeomorphic framework using stationary Gaussian kernels (GMM diff). We generated smooth random deformations by producing Gaussian random vector fields and convolving them with a Gaussian kernel. Then, we used the vector field exponential operator [11] to obtain a set of diffeomorphisms. We applied each diffeomorphism to our particle set transforming the points and the particle shapes according to section 2.3. Finally, we registered each set to the original template and quantified the registration error by taking the mean squared error (MSE) between each registered particle and the original position of the particle in the template. In fig. 2 we show the original template, the two deformed cases and the quantitative results for our registration comparison. Our method proved to perform better as it had an MSE of $0\ 185mm \quad 0\ 31mm^2$ lower than the diffeomorphic GMM: $0\ 245 \quad 084$ and GMM [5]: $0\ 261 \quad 095mm^2$.

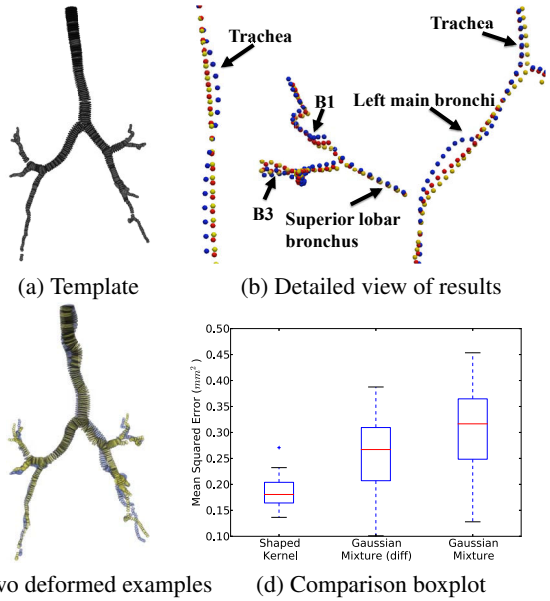

(a) Template (b) Detailed view of results

(c) Two deformed examples (d) Comparison boxplot

Fig. 2: Synthetic experiment results. (a) Airway tree template. (b) Detailed view with anatomy annotations. Ground truth (yellow), deformed airway with our approach (red) and GMM result (blue). It is worth noting how our approach achieves a better registration in the trachea and main bronchus. (c) Two randomly deformed examples. (d) Quantitative comparison showing that our method has a lower MSE than GMM when using our deformation model (diff) and than [5]

Human Data Airway Experiments We analyzed 20 volumetric chest CT datasets acquired at full inspiration (10 normal controls and 10 GOLD 4 COPD disease stage). The scans were performed either with GE scanner and Siemens scanners. In-plane pixel spacing ranged from 0.54mm to 0.85mm across all scans. The CT were down-sampled with a x4 ratio and the airway tree extracted using scale-space particles [3]. We show the results of our registration algorithm in the top right image of fig. 3.

As a proof-of-concept, we performed a statistical analysis on characteristic deformations of COPD which we show in fig. 4. We calculated the Jacobian determinant image at

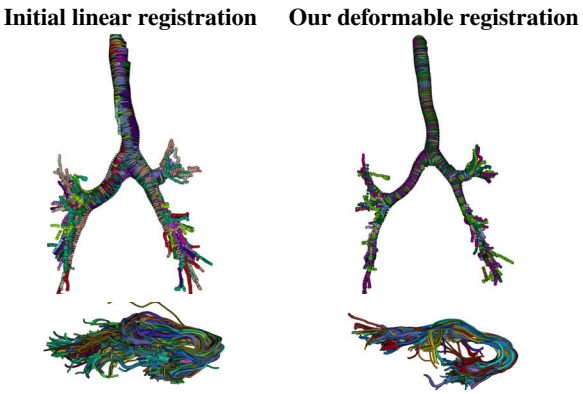

Fig. 3: Human data results. **Top row:** Airway trees from 20 subjects registered using our algorithm. **Bottom row**: 43 white matter tracts registered with our method. In both rows, each color indicates a different subject.

a resolution of $0\ 5mm^3$ for each of the diffeomorphisms obtained in the previous step. Then we used permutation based testing [12] in order to look for significant changes in the deformation without assuming hypothesis on the distribution of the Jacobian determinants. We found an area in which the trachea of the patients is significantly enlarged with a t-score of $1\ 5$ and a p-value$<\ 05$.

Human Data White Matter Tract Experiments Diffusion-weighted images from 43 subjects were acquired on a GE Signa HDxt 3.0T scanner using an EPI sequence of 51 directions with b=900 s/mm2, and 8 with b=0 s/mm2, with voxels of $1\ 7mm^3$. The left uncinate fasciculi were tracked by experts using 3D Slicer (www.slicer.org). We registered all the tracts with our algorithm. We show the result in fig. 3, where we can observe the consistency of the registered dataset.

4. CONCLUSION

In this work we present a method for registering point-sets endowed with a kernel function that defines the "shaped" of the point within a symmetric diffeomorphic transformation space. We tested our algorithm in synthetic and human datasets and we performed a statistical study on the deformation fields to illustrate the applicability of our algorithm showing improvement over current stationary techniques. There are other options exploiting non-stationary information: 1) When it is necessary to include in orientation in the model, like orientable surfaces or curves, the currents [13] approach is an interesting option. Our application cases however, do not need to model orientation. 2) Other approach recently proposed is restricting the deformation fields instead of changing the similarity metric [14], however no-current registration algorithm employs it. Finally, our approach may directly take advantage of information provided by the algorithms that extract point-set representations of anatomical structures [3] in order to shape each point in the set.

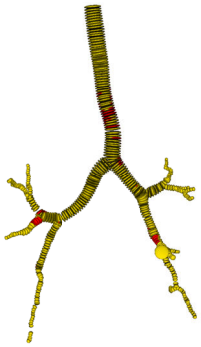

Fig. 4: Statistical analysis projected on the template: areas showing a compression in the COPD population are marked in red ($p \quad value < 0\ 05$).

5. REFERENCES

[1] P J Basser, S. Pajevic, C. Pierpaoli, J. Duda, and A. Aldroubi, "In vivo fiber tractography using DT-MRI data," *MRM*, 2000.

[2] S.R. Aylward and E. Bullitt, "Initialization, noise, singularities, and scale in height ridge traversal for tubular object centerline extraction," *IEEE TMI*, 2002.

[3] Gordon L. Kindlmann, R.S.J. Estepar, S.M. Smith, and Carl-Fredrik Westin, "Sampling and Visualizing Creases with Scale-Space Particles," *IEEE Viz*, 2009.

[4] Yanghai Tsin and Takeo Kanade, "A Correlation-Based Approach to Robust Point Set Registration," in *ECCV*, 2004.

[5] Bing Jian and Baba Vemuri, "Robust Point Set Registration Using Gaussian Mixture Models," *IEEE PAMI*, 2011.

[6] SC Joshi and MI Miller, "Landmark matching via large deformation diffeomorphisms," *IEEE TIP*, 2000.

[7] B. Avants, C.L. Epstein, M. Grossman, and James C. Gee, "Symmetric diffeomorphic image registration with cross-correlation: Evaluating automated labeling of elderly and neurodegenerative brain," *MIA*, 2008.

[8] G.E. Christensen and H J Johnson, "Consistent image registration," *IEEE TMI*, 2001.

[9] A.M. Peter and A. Rangarajan, "Information Geometry for Landmark Shape Analysis: Unifying Shape Representation and Deformation," *IEEE PAMI*, 2009.

[10] H. Guo, A. Rangarajan, S. Joshi, and L. Younes, "Non-rigid registration of shapes via diffeomorphic point matching," in *ISBI*, 2004.

[11] T Vercauteren, X Pennec, A Perchant, and N Ayache, "Symmetric Log-Domain Diffeomorphic Registration: A Demons-Based Approach," in *MICCAI*, 2008.

[12] T E. Nichols and A P. Holmes, "Nonparametric permutation tests for functional neuroimaging: a primer with examples," *HBM*, 2002.

[13] S Durrleman, X Pennec, A Trouvè, and N Ayache, "Statistical Models of Sets of Curves and Surfaces based on Currents," *MIA*, 2009.

[14] Laurent Younes, "Constrained Diffeomorphic Shape Evolution," *F. Comp. Math.*, 2012.